Global J. Environ. Sci. Manage. 7(4): 523-542, Autumn 2021

Global Journal of Environmental Science and Management
(GJESM)

Homepage: https://www.gjesm.net/

ORIGINAL RESEARCH PAPER

Estimation and mapping of the contribution of nitric acid to atmospheric corrosion of zinc

J.O. Castillo-Miranda[1,*], F.J. Rodríguez-Gómez[1], J. Genescá-Llongueras[2], L.G. Ruiz-Suárez[3], J.A. García-Reynoso[3]

[1]Departamento de Ingeniería Metalúrgica, Facultad de Química, Universidad Nacional Autónoma de México, Circuito Exterior s/n, Ciudad Universitaria, C.P. 04510, Ciudad de México, México

[2]Polo Universitario de Tecnología Avanzada, Universidad Nacional Autónoma de México, Vía de la Innovación 410 PIIT Autopista Monterrey-Aeropuerto Km. 10 C.P. 66629, Apodaca, Nuevo León, México

[3]Centro de Ciencias de la Atmósfera, Universidad Nacional Autónoma de México, Circuito de la Investigación Científica, Ciudad Universitaria, C.P. 04510, Ciudad de México, México

ARTICLE INFO

Article History:
Received 04 January 2021
Revised 09 April 2021
Accepted 24 April 2021

Keywords:
Air pollution
Damage to materials
Geographic information systems (GIS)
Multi-pollutant function
Urban atmosphere

ABSTRACT

BACKGROUND AND OBJECTIVES: Atmospheric zinc corrosion in the Mexico City Metropolitan area has long been attributed mainly to the effect of pollutants such as sulfur dioxide. There are changes in the urban atmosphere's chemical composition due to the implementation of air quality policies focused on reducing the emission of sulfur dioxide and other pollutants. This study's objectives were to estimate and map the contribution of nitric acid on zinc's atmospheric corrosion process.
METHODS: The impact of nitric acid on zinc is feasible to estimate using a function for a multi-pollutant situation. This function contemplates the sum of two contributions: one of nitric acid and another that includes sulfuric acid and climatic parameters. The multi-pollutant function is suitable to apply in areas without the strong influence of chlorides and tropical and subtropical climates, comparable to the Mexico City Metropolitan area.
FINDINGS: The results showed that spatial and temporal estimation of corrosion rates in grams per square meter of zinc was made for 2015-2019, using data modeling in a geographic information system. The maps of corrosion rates allowed us to visualize that, in general, the "southwest" zone has the most significant effects and that the lowest corrosion rates were presented in 2019 as an outcome of the implementation of air quality programs. Furthermore, a contribution of nitric acid up to 32% to the zinc corrosion rate was estimated.
CONCLUSION: The construction of corrosion rate maps provides a spatial and temporal estimate that allows visualizing areas where zinc materials are at risk corrosion due to the dispersion of atmospheric pollutants and climatic parameters. Likewise, it can represent a decision-making tool for the implementation of atmospheric corrosion studies of materials.

DOI: 10.22034/gjesm.2021.04.03

NUMBER OF REFERENCES	NUMBER OF FIGURES	NUMBER OF TABLES
74	6	3

*Corresponding Author:
Email: *j9lechatelier@yahoo.com.mx*
Phone: +52 55562 25225
Fax: + 52 55562 25228

Note: Discussion period for this manuscript open until January 1, 2022 on GJESM website at the "Show Article.

INTRODUCTION

The atmospheric corrosion process of hot-dip zinc-coated steel occurs in environments influenced by industrial activities with emissions of sulfur dioxide (SO_2), nitrogen oxides (NOx), and hydrogen sulfide (H_2S). In marine environments, the reaction occurs with chlorides, together with carbon dioxide (CO_2) and water (H_2O) (Friel, 1986). The hydrogen potential (pH) of the aqueous surface film depends on the atmospheric concentration of SO_2 and NOx, essential for the corrosion process because it controls the dissolution of the passive oxyhydroxide surface (Graedel, 1989; Graedel and Frankenthal, 1990). Corrosive atmospheric trace substances, such as SO_2, nitrogen dioxide (NO_2), and hydrogen chloride (HCl), accelerate metallic corrosion by acidifying the surface electrolyte and accelerate metal corrosion (Johansson, 1990). Knotková and Bartoň (1992) analyzed the contribution of acid deposition as a heterogeneous dynamic system of atmospheric corrosion metals. Kucera and Fitz (1995) considered that an acid effect in the atmosphere due to a multi-pollutant situation was the cause of the damage to materials. The deterioration of various materials, to some extent, is caused by acid gases such as SO_2, nitric acid (HNO_3), and HCl (Ferm *et al.,* 2005). Current studies indicate that the corrosion effect of HNO_3 exceeds SO_2, with a factor between 2 and 20 depending on the exposed material (Tidblad *et al.,* 2009). Atmospheric corrosion metals has long been attributed to SO_2 and chlorides (Cl^-), which has been demonstrated in laboratory weathering exposures and proven in field exposures. So, the promulgation of environmental protection laws in industrialized countries, in addition to the efforts inside the limits of the Convention of the United Nations Economic Commissions for Europe (UN ECE) on Long-range Transboundary Air Pollution (CLRTAP), led to a notable decrease in SO_2 levels. However, the concentration levels of other air pollutants, such as NOx and ozone (O_3), remained or even increased slightly. Therefore, the effect of SO_2 needs to be considered in a multi-pollutant situation with other polluting gases such as NO_2 and O_3, including particles (Oesch and Faller, 1997; Tidblad *et al.,* 2002a). The levels of environmental concentration for HNO_3 are lower concerning SO_2; however, depending on the aggressiveness, HNO_3 can be compared to SO_2 in a multi-pollutant situation (Tidblad *et al.,* 2009). Atmospheric sulfur levels have been better controlled, and there has been a considerable reduction in SO_2 emissions, while the concentration of NOx and HNO_3 has increased due to emissions from automobile traffic (Graedel and Frankental, 1990; Pantani *et al.,* 1998). HNO_3 has higher concentrations in urban areas than in rural areas, but they are lower than NO_2 in urban areas (Ferm *et al.,* 2005). The current study's main objective is to estimate nitric acid's spatial and temporal contribution to zinc's atmospheric corrosion in the Mexico City Metropolitan Area (MCMA) for 2015-2019., Maps of corrosion rates in grams per square meter (g/m^2) were constructed to achieve this objective. Also, the maps provide a spatial estimate of the corrosion risk of zinc materials when exposed to a polluted atmosphere. This study was carried out in the Mexico City Metropolitan Area in 2020.

The behavior of HNO_3 in the atmosphere of the Mexico City Metropolitan area

The Mexico City Metropolitan Area (MCMA) is located between north 19° 03' to 19° 54' latitude and 98° 38' to 99° 31' west longitude. It is part of an endorheic basin, with an average altitude of 2,240 meters above sea level. It is in the "East" area of the region known as the Transverse Neovolcanic System. The latitude of the MCMA can accelerate the photochemical reactions of pollutants in the atmosphere due to intense solar radiation. Likewise, there are anticyclonic systems in the area that keep the sky clear and increase the photochemical capacity of the atmosphere (SMA, 2008). MCMA is one of the largest megacities worldwide, as it has a population of more than 21 million people (UN, 2016). MCMA lies in central Mexico, at a tropical latitude where the climate is semi-dry temperate tropical in the northeast region; in the center, the temperate subhumid predominates, and in the upper, semi-cold subhumid type regions. Generally, the main entry of wind is located in the north, although there may be wind flow from south to north (Jáuregui, 2000; INEGI, 2007). The rainy season with high relative humidity occurs from May to October (Jáuregui and Romales, 1996), causing the levels of some pollutants to drop due to atmospheric instability. The upper levels of precipitation are registered in the mountainous areas and the lowest mainly in the northeast (INEGI, 2007). A study of the chemical composition of rain samples in Mexico City through multiple regression

analysis for the period 1994-2000 showed that the contribution of Cl^- (chloride-based sea salt) with sodium ion (Na^+) and potassium ion (K^+) was 2.2 percentage (%) at the prediction of the hydrogen ion (H^+) concentration. It allows us to assume that the chlorides found in rainwater come from sources other than sea salt. Likewise, Mexico City is placed at more than 300 kilometres (km) from the nearest shore, surrounded by high mountains. The Sierra Madre Oriental, with mountains above 4000 meters above sea level, is located near the Gulf of Mexico coast, where heavy rains are produced that intervene in further eliminating sea salt aerosols (Báez *et al.,* 2006). A study of the humid atmospheric deposition in the 2013-2016 period in the MCMA indicated that the calcium Ca^{2+} and Cl^- ions represented total annual deposits of 8% to 9% and 3% to 8% (Avila, 2018). The presence of chlorides could be attributed to emissions of approximately 30,000 small, medium, and heavy industries located in the northern part of the MCMA and the residential use of hypochlorite. There are hypochlorite production, ferrous and non-ferrous foundries, glass producers, motor vehicle manufacturers (a foundry), automobile assembly, plant factories, lime, brick, ceramics, cement, and tires (García *et al.,* 2009). The altitude of the MCMA leads to a lower oxygen content of the air, approximately 23% lower than at sea level. It causes the combustion processes to operate poorly and diffuse a greater quantity of pollutants into the atmosphere, together with the surrounding mountain chain, which favors its stagnation (Molina and Molina, 2002). In 2016, Mexico City registered 2.3 million vehicles; the most abundant are those for private use, such as cars, Sport Utility Vehicle (SUVs), and motorcycles, which account for 83% of the total fleet. Total emissions of nitrogen oxides from this vehicle fleet represented a total of 60,907 Megagrams per year [Mg/y], with private cars and trucks being the main generators with an amount of 52,437 [Mg/y], which represents 86% of the total (SEDEMA, 2018a). The concentrations of SO_2 and NO_2 in the ambient air remained during 2017 below the limit concentrations required by the Official Mexican Environmental Health Standards. The Tula-Tepeji corridor remains the most important source of sulfur dioxide for Mexico City. An analysis of the trend indicated that since 2000, SO_2 concentrations maintained a downward trend, while nitrogen oxides did not show a significant trend. NO_2 contributes about 60% of the total concentration of nitrogen oxides. Also, acid rain samples were recorded in the rainy season at places south and east of Mexico City (SEDEMA, 2018b). Studies on the monitoring of the atmospheric concentration of HNO_3 in the MCMA and its spatial distribution are scarce. HNO_3 shows a behavior similar to ozone, reaching a maximum level during the day and a low level at night. Also, it tends to increase its concentration from north-northeast to south-southwest (Moya *et al.,* 2004; Zheng *et al.,* 2008; Wood *et al.,* 2009; Cuevas, 2014). A map of the annual average concentration of HNO_3 micrograms per cubic meter ($\mu g/m^3$) for the year 2007 shows that the highest concentration levels are located in the northwest area of the MCMA (Castillo-Miranda *et al.,* 2017). The climatic conditions in the MCMA area are as follows: In 2015, average temperature 16.4 °C. April hottest 18.7 °C. Relative humidity (RH) average 62%, atypical rain during march and April (35 and 17 mm). Average precipitation 672 millimeters (mm). Barometric pressure average 584 milimeters of mercury (mmHg) (581-588 interval). Average wind speed 2.0 meters per second (m/s), highest values during October 2.3 m/s (SEDEMA, 2016). In 2016, average temperature 16.2 °C, May hottest 19.5 °C. RH 57% average. Average precipitation 965 mm. Barometric pressure average 585 mmHg (575 - 591 interval). Average wind speed 2.1 m/s (SEDEMA, 2017). In 2017, average temperature 16.8 °C, May hottest 19.7 °C. RH 54% average. Average precipitation 965 mm. Barometric pressure average 585 mmHg (580 - 591 interval). Average wind speed 2.1 m/s (SEDEMA, 2018c). In 2018, average temperature 16.7 °C, May hottest 19.4 °C. RH 57.1% average. Average precipitation 786.2 mm. Barometric pressure average 584.9 mmHg (583 - 589 interval). Average wind speed 2.0 m/s (SEDEMA, 2020b). In 2019, average temperature 17.4 °C. RH 53.2%, Average precipitation 565.3 mm. Average wind speed 2.1 m/s (CONAGUA, 2019). For pollutant SO_2 has a reduction between 2015 to 2019 from near 70 parts per billion (ppb) go 47 ppb. In case of the NO_2 from near 130 ppb to 110 ppb (SEDEMA, 2020c).

Effects of nitric acid on zinc corrosion

In the modern urban atmosphere, the concentration levels of SO_2 tend to decrease, increasing the relative importance of other trace gases such as NO_2. The importance of NO_2 lies in being the

precursor of HNO_3 that participates in the materials' degradation processes (Graedel and Schwartz, 1977; Svensson and Johansson, 1993). HNO_3 is a molecule that quickly adsorbs to surfaces, specifically if there is water on the surface. Due to its high solubility in water, HNO_3 is rapidly deposited on surfaces and in water droplets (Seinfeld and Pandis, 2016; Finlayson-Pitts and Pitts Jr., 2000). It experiences dry and wet deposition rapidly, with deposition rates in the range of 1-5 cm/s (Finlayson-Pitts and Pitts Jr., 2000). The atmospheric removal processes for nitric acid gas are by wet and dry deposition. The estimated half-life for dry and wet nitric acid deposition is 1.5 to 2 days and 2 to 3 days, respectively. There is also an efficient removal of nitric acid during precipitation events (Hamilton and Crabbe, 2009). Laboratory studies (Edney and Stiles, 1986; Svensson and Johansson, 1993) have been conducted on the effect of SO_2, NOx, and oxidants on the early stages of the galvanized steel atmospheric corrosion. This corrosion is due to the dry deposition of SO_2 and HNO_3, and HNO_3 is likewise a source of wet NO_3 (Edney *et al.,* 1986). They also found that the deposition rate was 0.02 centimeter per second (cm/s) for NO_2, and HNO_3 was 2.0 (m/s). The only relevant role of atmospheric nitrogen is likely to serve as an acidifying species in the precipitation and deposited aerosol particles, as shown in Fig. 1.

Nitric acid is the main gaseous component that dissolves in the aqueous surface layer, and nitrates come from both particles and the quantity of precipitation. Trace amounts of nitrates in the zinc corrosion layers were discovered, and it was possibly zinc nitrate ($Zn(NO_3)_2$) (Graedel, 1989). Friel (1986) obtained nitrate ions in low concentrations from the zinc corrosion layers. Oesch and Faller (1997) reported the formation of basic zinc nitrate $Zn_5(NO_3)_2(OH)_8 \cdot 2H_2O$, which is formed when zinc is exposed to parts per million (ppm) levels of NO_2. HNO_3 has a very high dry deposition rate (V_d) that is generally independent of relative humidity and is rapidly adsorbed on most surfaces, making it relatively more harmful for dry and hot climates (Kucera, 2003; Tidblad *et al.,* 2012). Deposited nitrate particles are associated with coarse particles. These coarse particles are commonly alkaline and can also contain sodium chloride. This composition makes them a sink for nitric acid. The reaction can be carried out in the atmosphere or deposited particles (Tidblad *et al.,* 2012). Laboratory experiments and data from the literature show that the relatively high (V_d) of HNO_3 has mainly been attributed to the extreme adherence and reactivity of HNO_3 (Samie, 2007b). Also, the solubility of HNO_3 in water, according to Henry's law coefficients (2.1 x 10^5 mole per liter atmosphere (mol/L atm), is higher than SO_2 and NO_2, which have 1.24 and 0.01 mol/L atm, respectively (Seinfeld and Pandis, 2016; Oesch, 1996). It allows a high solubility of HNO_3 in the electrolytic layer and increases the corrosion rate (Samie *et al.,* 2007b). HNO_3 is soluble in water,

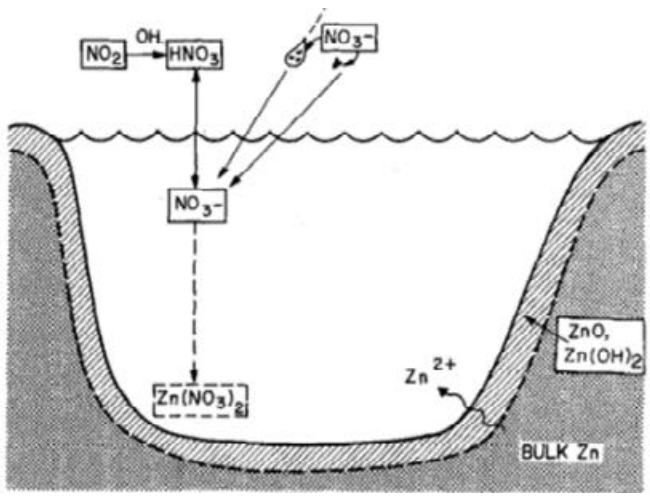

Fig. 1: A schematic representation of the processes involved in the formation of components containing nitrogen during the atmospheric zinc corrosion (Graedel, 1989)

and the concentration in urban environments is relatively low (1-4) µg/m^3 compared to SO_2 (1-20) µg/m^3. Nitrate salts (NO_3^-) are formed when metals react with HNO_3; however, nitrate salts are soluble in water, and this may be one reason for the rare occurrence of nitrates in layers of corrosion products (Samie *et al.,* 2007a). Pure zinc plates were exposed in the field for a year, within the Model for Multi-pollutant Impact and Assessment of Threshold Levels for Cultural Heritage (MULTI-ASSESS) and Regional Air Pollution in Developing Countries (RAPIDC) programs in Europe, Asia, and Africa. The Fourier transform spectroscopy (FTIR) technique demonstrated the presence of nitrates as corrosion products. Likewise, nitrates with high solubility are found in greater quantity on the plate's backside since they are less affected by precipitates. Furthermore, essential nitrates ($Zn_5(NO_3)_2(OH)_8 \bullet 2H_2O$) are generally more soluble in acidic solutions than in water. Therefore, the pH decreases in the absorption layer when acidic contaminants dissolve. Consequently, the essential nitrates are dissolved and removed from the surface by the presence of rain. Accordingly, the zinc front side corrodes more because it has a less protective layer of basic nitrate (Samie *et al.,* 2007a).

Damage functions

The development of various exposure studies has shown that atmospheric corrosion is a phenomenon that varies considerably in each locality (Guttman and Sereda, 1968). The development and use of a damage function applying the fundamental principles of thermodynamics and kinetics of atmospheric corrosion allow predicting galvanized steel structures corrosion rates due to dry and wet deposition (Spence and Haynie, 1990). The dose-response functions should reflect the physicochemical nature of atmospheric corrosion and each parameter's contribution to the global effect (Leuenberger-Minger *et al.,* 2002). Since atmospheric corrosion affects all structures exposed to potentially corrosive environments, many countries have established programs dedicated to understanding and monitoring (Roberge *et al.,* 2002). In some cases, atmospheric exposure programs are conducted to assess the corrosivity of specific atmospheres. This type of information can help choose coatings or corrosion protection systems at particular sites (Dean Jr., 2005). A set of exhibition programs such as International testing program [] (ISOCORRAG), Ibero-American Map of Atmospheric Corrosiveness (MICAT), International Co-operative Programme on Effects on Materials, including Historical and Cultural Monuments (ICP materials), Model for Multi-pollutant Impact, and MULTI-ASSESS and RAPIDC have been developed in the last decades in different parts of the world. The International Testing Program (ISOCORRAG) began in 1987-1989 with International Organization for Standardization/Technical Committees 156 (ISO/TC 156) test methods and procedures to provide environmental and corrosion data. It includes 53 test sites in 14 countries located in Europe, Argentina, Canada, Japan, New Zealand, and the United States (Knotková, 1993). However, the ISOCORRAG and MICAT programs lack data on gases other than SO_2 and wet deposition (Tidblad *et al.,* 2009). However, atmospheric corrosivity can be estimated with consistent environmental information to establish damage functions, based on a statistical analysis of the databases' information (Morcillo *et al.,* 2002). The ICP Materials program had its first stage (1987–1995), where dose-response functions were developed with long-term data on corrosion and contamination to investigate the effect of acid deposition on materials. It includes non-marine sites, lacks data on the dry deposition of chlorides and HNO_3 and particles. In this period, SO_2 concentrations were still relatively high but decreasing. It led to the need for a new multi-pollutant exposure program (1997–2001). This program aimed to determine both the effect of SO_2 and other important air pollutants such as HNO_3 and particles. In the 2002-2003 period, the MULTI-ASSESS project included HNO_3 and particles as mandatory parameters (Tidblad *et al.,* 2012). Also, RAPIDC project included measurements of HNO_3 and particulate matter. Also, the program was set up with 18 sites in the South and Southeast of Asia and South Africa, which have tropical and subtropical climates. Both the MULTI-ASSESS Program and RAPIDC are the most suitable for investigating the effects of multiple pollutants in non-marine environments (Tidblad *et al.,* 2009). After one year (2002-2003), zinc RAPIDC exposure's corrosion is lower than expected compared to values calculated (Tidblad *et al.,* 2007) using the best available dose-response functions. However, due to the relatively high measured SO_2 levels, it was correct to use functions for the dominant SO_2 situation developed within the ICP Materials program (Tidblad

et al., 2001). The International Organization for Standardization (ISO) ISO 9223 standard is intended to evaluate the corrosivity category for metals. This category explicitly describes the corrosiveness of outer atmospheres through the development of dose-response functions. Considering the above, the dose-response function for zinc is supported on data after one year of exposure. It can, therefore, only be used for classification objects (Zn, N=116, R^2=0.78), using Eq. 1 (Tidblad *et al.,* 2002b).

$$C_{Zn} = 0.0053\ SO_2^{\ 0.43}\ TOW^{0.53} \exp\{f_{Zn}\} + 0.00071\ Cl^{0.68}\ TOW^{0.30} \exp\{0.11T\} \quad (1)$$

$$f_{Zn}\ (T) = 0 \text{ when } T \leq 10\ °C, \text{ otherwise } -0.032(T-10)$$

Where;

C_{Zn} = Corrosion attack after 1 year of exposure in µm of zinc; T=Temperature in °C; TOW=Time of wetness in hour per year (h/y); SO_2= SO_2 deposition in milligram per square meter day (mg/m^2day); Cl= Cl^- deposition in mg/m^2/day.

Corrosivity mapping

Mapping the regional distribution of corrosivity is a method that provides general information on corrosion, rational use, and selection of material protection measures. The mapping must be based on the knowledge of the deterioration and kinetic processes based on external factors, and it generalizes the information supported on local environmental conditions. Likewise, it requires available information on the levels of atmospheric environmental components and converts it into values on the effects of corrosion. The above is achieved using damage equations (dose-response functions) obtained from empirical procedures applied to data processing using GIS technologies (Knotková and Kreislova, 2007). The classification of the different atmospheric basins based on corrosivity serves to select optimal metallic materials and coatings for adequate protection against corrosion in a country (Genescá and Rodríguez, 1992). The atmospheric corrosion maps for metals in Mexico were designed according to the ISO 9223 classification system. They required annual mean corrosion values in test stations, meteorological data, and atmospheric pollution such as SO_2 and chloride ions (Cl^-) (Mariaca *et al.*, 1999). Corrosivity maps were constructed for zinc, copper, and aluminum in the MCMA, by characterizing the atmospheric aggressiveness on these materials based on the ISO 9223 standard. Furthermore, atmospheric aggressiveness does not necessarily correspond to the most polluted areas since it depends on the relative humidity and wetting time (Muñoz and Uruchurtu, 2002).

MATERIALS AND METHODS

Selection of the dose-response function

The dose-response functions are empirical expressions and then simplifications that indicate the relationship between the rate of corrosion or deterioration and the levels of pollutants combined with climatic parameters (Kucera, 2004). At first, the dose-response functions were more focused on SO_2, as the main stimulator of corrosion. These functions were denoted as dose-response functions for the dominant SO_2 situation. However, as there have been changes in the atmosphere's chemical composition, there are higher levels of concentration of nitrogen, ozone, and particles than of SO_2. The above made it possible to propose "multi-pollutant" type functions. Multi-pollutant functions are preferable at high levels of particulate and nitrogen pollutants in the air. The above occurs in urban atmospheres dominated by traffic (Kucera, 2005). Other important factors in applying the multi-pollutant dose-response function are chloride concentration [Cl^-] and Temperature (T). This function is applicable in geographic areas without the influence of chlorides, have been developed and suggested to be implemented in countries with tropical and subtropical climates, characteristic of the MCMA. Likewise, in these climates, the corrosion rate of zinc in field tests consisting of a rack for placing zinc samples and holding passive samplers for gases is lower compared to the corrosion rates obtained with the best available dose-response functions (Tidblad *et al,* 2007). Table 1 shows the annual average concentration levels of SO_2, NO_2, and Cl^- and the yearly average temperature obtained from the monitoring stations located in the MCMA in the period 2015-2019 (SEDEMA, 2020a). The concentration levels of SO_2, in general, are low and are more noticeable for the year 2019. The concentration levels of NO_2 are higher than SO_2. The Cl^- concentration is less than 5 milligrams per liter (mg/L), and the temperature is greater than 10 °C, which suggests the use of a multi-pollutant dose-response function that includes the effect of HNO_3.

Table 1: Measurements of [SO_2], [NO_2], [Cl^-] and T annual average in the period 2015-2019

Parameter	Year				
	2015	2016	2017	2018	2019
SO_2 (µg/m^3)	8.45	8.48	9.63	8.54	6.87
NO_2 (µg/m^3)	36.46	35.28	36.61	36.30	31.58
Cl^- (mg/L)	0.45	0.29	0.25	0.24	0.21
T (°C)	16.51	16.42	16.44	16.26	17.17

Dose-response functions are importantly applied to map areas of increased risk corrosion and to calculate corrosion costs. Furthermore, it is possible to estimate the loss of mass of zinc for a multi-pollutant situation (Kucera *et al.*, 2007). The statistical processing of data from materials exposed in the field generated a dose-response function for the loss of zinc mass after one year of exposure, using Eq. 2 (Kucera, 2005).

$$ML = 3.53 + 0.471[SO_2]^{0.22} e^{0.018RH+f(T)} + 0.041Rain [H^+] + 1.37[HNO_3] \quad (2)$$

$f(T) = 0.062(T-10)$ when $T \leq 10^{\circ}C$,
$f(T) = -0.021(T-10)$ otherwise

Where ML is the corrosion rate in g/m^2, [SO_2] and [HNO_3] is the concentration in micrograms per cubic meter (µg/m^3), RH is the relative humidity in %, Rain is the amount of precipitation in millimeters (mm), [H^+] is the H^+ concentration of rainfall in mg/L, and T is the temperature in °C. Eq. 2 shows an evident effect of HNO_3 on zinc corrosion and represents the sum of two contributions, one from HNO_3 and the other from corrosion-enhancing factors including SO_2 (Samie et al, 2007a). They also found a relatively good correlation between the extrapolated zinc mass loss, based on laboratory exposures, and the dose-response function based on a statistical analysis of field data. The multi-pollutant function includes nitric acid that any MCMA monitoring station does not measure. Eq. 3 developed within the MULTI-ASSESS project can be used to calculate the annual concentration of HNO_3 when there are no values (Kucera, 2005):

$$[HNO_3] = 516 \bullet e^{-3400/(T+273)} ([NO_2] \bullet [O_3] \bullet RH)^{0.5} \quad (3)$$

Where [HNO_3], [NO_2] and [O_3] is the concentration in µg/m^3; RH is the relative humidity in %, and T is the temperature in degree Celsius (°C). The oxidation process from NO_2 to HNO_3 described in equations (4-21) contemplates the chemical species of Eq. 3.

The NO_2 molecule absorbs sunlight at wavelengths <430 nm and can break one of the NO bonds and generate the reactive ground-state oxygen atom, the triplet-P oxygen atom, O (^{3}P), and a NO molecule, using Eq. 4 (Seinfeld, 1980).

$$NO_2 + h\nu \rightarrow NO + O(^3P) \quad (4)$$

The exceptionally reactive triplet-p oxygen atom formed regularly collides with oxygen molecules to form ozone, using Eq. 5.

$$O(^3P) + O_2 + M \rightarrow O_3 + M \quad (5)$$

Under typical polluted atmosphere conditions, the ozone molecule will often react with NO to regenerate NO_2, using Eq. 6.

$$O_3 + NO \rightarrow NO_2 + O_2 \quad (6)$$

Ozone can also photolyze, using Eqs. 7 and 8.

$$O_3 + h\nu \xrightarrow{280\text{-}350\ nm} O_2(^1\Delta, {}^3\textstyle\sum) + O(^1D, {}^3P) \quad (7)$$

$$O_3 + h\nu \xrightarrow{450\text{-}700\ nm} O_2(^1\Delta, {}^3\textstyle\sum) + O(^3P) \quad (8)$$

The singlet-D oxygen atom is considerably more reactive than the ground-state triplet-P oxygen atom, using Eq. 9. Apart from deactivation.

$$O(^1D) + M \rightarrow O(^3P) + M \quad (9)$$

It reacts with water to form the hydroxyl radical, using Eq. 10.

$$O(^1D) + H_2O \rightarrow 2OH\cdot \quad (10)$$

Ozone can react with nitrogen dioxide to produce

symmetrical nitrogen trioxide, using Eq. 11.

$$O_3 + NO_2 \rightarrow NO_3 + O_2 \quad (11)$$

The NO_3 species forms dinitrogen pentaoxide, by reaction with nitrogen dioxide, using Eq. 12.

$$NO_3 + NO_2 \rightarrow N_2O_5 \quad (12)$$

Dinitrogen pentaoxide can rearrange to form NO_3 and NO_2 or maybe react with water to form nitric acid, using Eqs. 13 and 14.

$$N_2O_5 \rightarrow NO_3 + NO_2 \quad (13)$$

$$N_2O_5 + H_2O \rightarrow 2HONO_2 \quad (14)$$

The subsequent reaction can take place between oxygen atoms and NO_2, using Eq. 15.

$$NO_2 + O(^3P) \rightarrow NO + O_2 \quad (15)$$

In addition, NO and NO_3 can react to regenerate NO_2, using Eq. 16.

$$NO_3 + NO \rightarrow 2NO_2 \quad (16)$$

Nitrous acid is generated by using Eq. 17.

$$NO + NO_2 + H_2O \rightarrow 2HONO \quad (17)$$

And can react bimolecular to regenerate the original reactants, using Eq. 18.

$$HONO + HONO \rightarrow NO + NO_2 + H_2O \quad (18)$$

Photolysis of nitrous acid in the wavelength range 280-400 nm guide to producing hydroxyl radical and NO, using Eq. 19.

$$HONO + hv \rightarrow OH\cdot + NO \quad (19)$$

The hydroxyl radical may react with NO and NO_2 to yield nitrous and nitric acid using Eqs. 20 and 21, respectively.

$$OH\cdot + NO \rightarrow HONO \quad (20)$$

$$OH\cdot + NO_2 \rightarrow HONO_2 \quad (21)$$

Applied method

Mapping of the corrosion rates was carried out through the following procedure: Integration of the available data from measurements of concentrations of sulfur dioxide (SO_2), estimated nitric acid (HNO_3), relative humidity (RH), rainfall, or amount of precipitation (PP), temperature (T) and the acidity of the rain [H^+]. The data and results were applied in suitable mathematical functions to construct, by interpolation, maps of their spatial distribution. Subsequently, with these values, the multi-pollutant function corresponding to zinc is applied to obtain the corrosion layers. A description of these steps is presented in the following paragraphs.

Damage function parameter database

The database was integrated with the multi-pollutant function parameters to calculate the corrosion rate in the period 2015-2019. These parameters are obtained from the different monitoring stations as described down below. For this study, SO_2 data generated by the Red Automática de Monitoreo Atmosférico (Automatic Atmospheric Monitoring Network, RAMA) for the period (2015-2019) are used. The estimation of HNO_3 required annual average values per hour of the parameters: Nitrogen dioxide (NO_2) and ozone (O_3) from the (RAMA); in addition to temperature (T) and relative humidity (RH) from the databases of the Red de Meteorología y Radiación Solar (Atmospheric Monitoring Network and the Meteorology and Solar Radiation Network, REDMET). The values of the acidity of the precipitation [H^+] and the amount of rainfall or rain (PP) included in the multi-pollutant function were obtained from data reported by the Red de Depósito Atmosférico (Atmospheric Deposit Network, REDDA) for the period (2015-2019). The values of temperature (T) and relative humidity (RH) included in the dose-response function were obtained from the database of the Red de Meteorología y Radiación Solar (Meteorology and Radiation Network, REDMET) for the period (2015-2019) (SEDEMA, 2020a).

Creating layers using geographic information systems
Selecting the interpolation method

Geographic information systems (GIS) are an indispensable technology for capturing, storing, analyzing, modeling and displaying spatially

referenced data (Moreno, 2006a). Conesa (1996) indicated that GIS could process large databases with information about the land surface globally and globally. One of a GIS's purposes is to provide a spatial framework to support decisions about the efficient use of the earth's resources and manage the anthropogenic environment (Zeiler, 1999). The kriging method combined with deterministic modeling improves the spatial analysis of acid deposition (Venkatram, 1988). Modeling temperature and relative humidity were interpolated using the kriging method, and the standard deviation (SD) was used to measure the spatial uncertainty (Phillips and Marks, 1996). The inverse distance weighting (IDW) and kriging spatial interpolation techniques are regularly used to estimate pollutant concentration levels in areas with limited sample points. The value of each parameter is determined by cross-validation until the least mean square error (RMSE) is obtained (Rojas-Avellaneda, 2007; Diem and Comrie, 2002). Pollutant concentration maps using the kriging method are used in the European Monitoring and Evaluation Materials Program (EMEP) (Denby *et al.,* 2005). Modeling the temporal behavior of SO_2 using the ordinary kriging method provides an estimate of the air quality in Europe. It is suggested to use a semivariogram with a spherical model to obtain the SO_2 layer (Denby *et al.,* 2010). In this study, spatial representation was developed using Aeronautical Reconnaissance Coverage Geographic Information System (ArcGIS) software (ArcGIS, 2014). ArcGIS uses the extension called "geostatistical analysis". It employs advanced tools to perform exploratory analysis of spatial data and a wizard with which statistical surfaces are constructed. The layers' construction was decided to build vector layers with both IDW and ordinary kriging for each of the parameters. The selection of the interpolation method for each parameter was based on obtaining the lowest value of the Root Mean Square (RMS) of the cross-validation. The coefficient of determination R^2 of the relationship observed value vs. predicted value resulting from the cross-validation is obtained. The ordinary kriging interpolation method was used to obtain the layers of the following parameters, with their corresponding annual coefficient of determination R^2: [SO_2]: 2015 = 0.60; 2016 = 0.52; 2017 = 0.76; 2018 = 0.71 and 2019 =0. 67. [HNO_3]: 2015 = 0.55; 2016 = 0.76; 2017 = 0.73; 2018 = 0.60 and 2019 = 0.60. HR: 2015 = 0.02; 2016 = 0.17 and 2018 = 0.15. T: 2015 = 0.44; 2016 = 0.60; 2017 = 0.41; PP: 2016 = 0.67; 2017 = 0.87; 2018 = 0.70 and 2019 = 0.72. [H^+]: 2017 = 0.01; 2018 = 0.20 and 2019 = 0.21. The IDW interpolation method was employed to obtain the following parameters' layers, with their corresponding annual coefficient of determination R^2: HR: 2017 = 0.03 and 2019 = 0.01. T: 2018 = 0.40 and 2019 = 0.32. PP: 2015 = 0.26. [H^+] 2015 = 0.09 and 2016 = 0.52.

RESULTS AND DISCUSSION

Layer maps of the parameters of the dose-response function and the corrosion rate

The representation of the maps of the dose-response function parameters focuses mainly on SO_2 as one of the main factors in the corrosion process and HNO_3 regarding corrosion in the urban atmosphere. The sulfur dioxide [SO_2] layers for the period 2015-2019 are shown in Fig. 2. The figure indicates spatially that the highest [SO_2] levels are located to the "northwest" and the lowest to the "east, northeast" and "southeast" and a lesser extent south of the MCMA. From a temporal perspective, the highest levels of [SO_2] are present in 2017 and 2018, while the lowest levels occur in the year 2019, followed by 2015 and 2016. The [HNO_3] layers for the period 2015-2019 are represented in Fig. 3. The figure shows spatially that the highest [HNO_3] levels are located in the "central" and "southwest" areas and the lowest in the "east" and "northeast" areas of the MCMA. From a temporal viewpoint, the highest [HNO_3] levels are in 2015 and 2016, while the lowest levels are in 2016, followed by 2018. The importance of the annual change in the levels of HNO_3 concentration observed in the maps allows visualizing the urban atmosphere's complexity in relation to its acidity.

The corrosion layers for zinc used in the evaluation were constructed using the "raster calculator" tool included in the ArcGIS 10.2.2 spatial analysis extension. It performs analysis operations with mathematical functions. The process consists of applying the multi-pollutant function, introducing the raster layers of the corresponding parameters. These layers represent the terrestrial space's property through a set of square cells of the same size, called pixels. The raster model is appropriate to represent continuous variables in space, such as meteorological variables and air pollution (Moreno, 2006b). The corrosion rate maps construction results are shown in Figs. 4 and 5.

The layers of the corrosion rates employing the multi-pollutant function of equation 2 for 2015-2019 are shown in Fig. 4. The images show a corrosion rate of 5.81-8.19 of mass loss (g/m^2). Spatially, the highest corrosion rates are located in the "southwest" of the MCMA. On the other hand, the lowest corrosion rates are seen in the "northeast-southeast" of the MCMA. The highest corrosion rates present in 2015 and 2016, while the lowest corrosion rate occurs in the year 2019. Likewise, the corrosion rates' layers using the

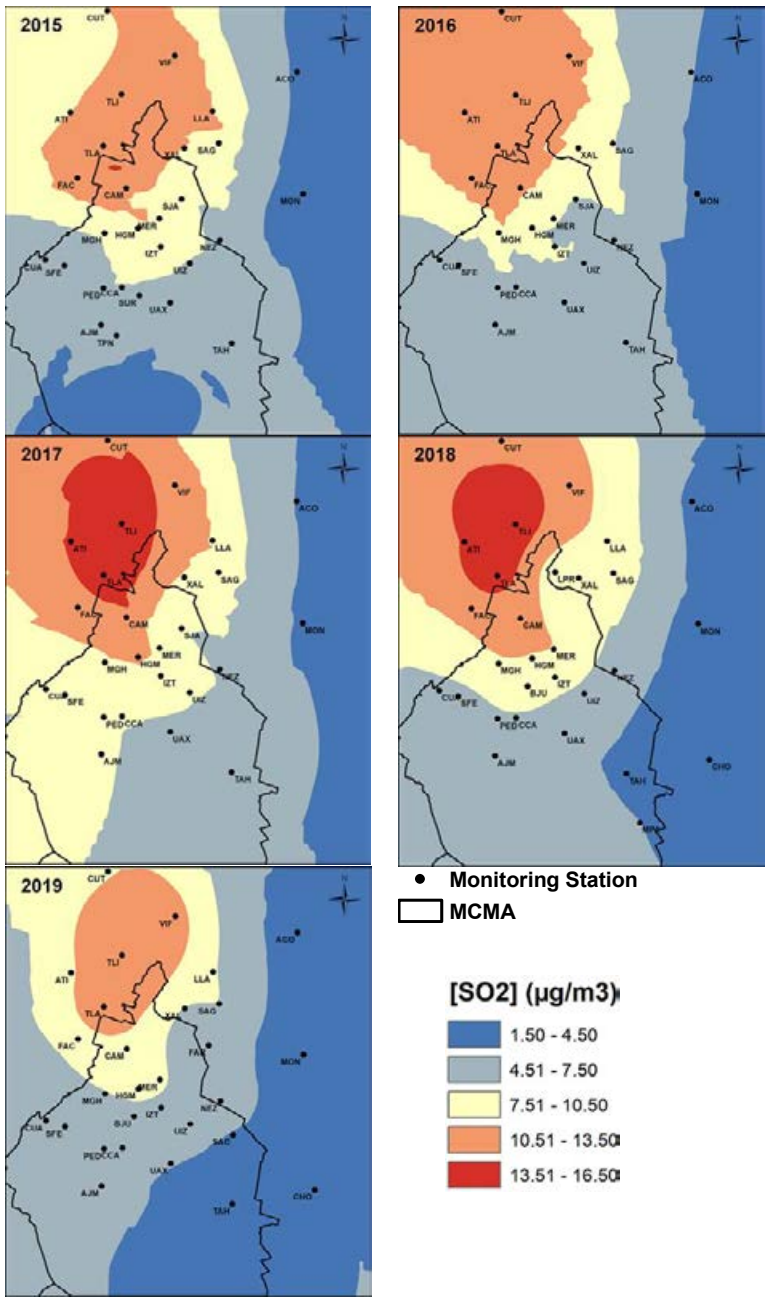

Fig. 2: Maps of concentration layers of the annual average of sulfur dioxide [SO_2] (µg/m^3) for the period 2015-2019 in the MCMA

multi-pollutant function of equation 2, without the component that includes HNO_3 for 2015-2019, are shown in Fig. 5. The images establish a corrosion rate interval of [4.86-6.64] of mass loss (g/m^2). Spatially, the corrosion rates represent the same trend as in Fig. 4. The highest rates are located in the "southwest" of the MCMA, although the area covered is smaller. Meanwhile, the lowest corrosion rates are seen in the "northeast-southeast" of the MCMA, covering larger areas. In the same way, temporarily, the highest

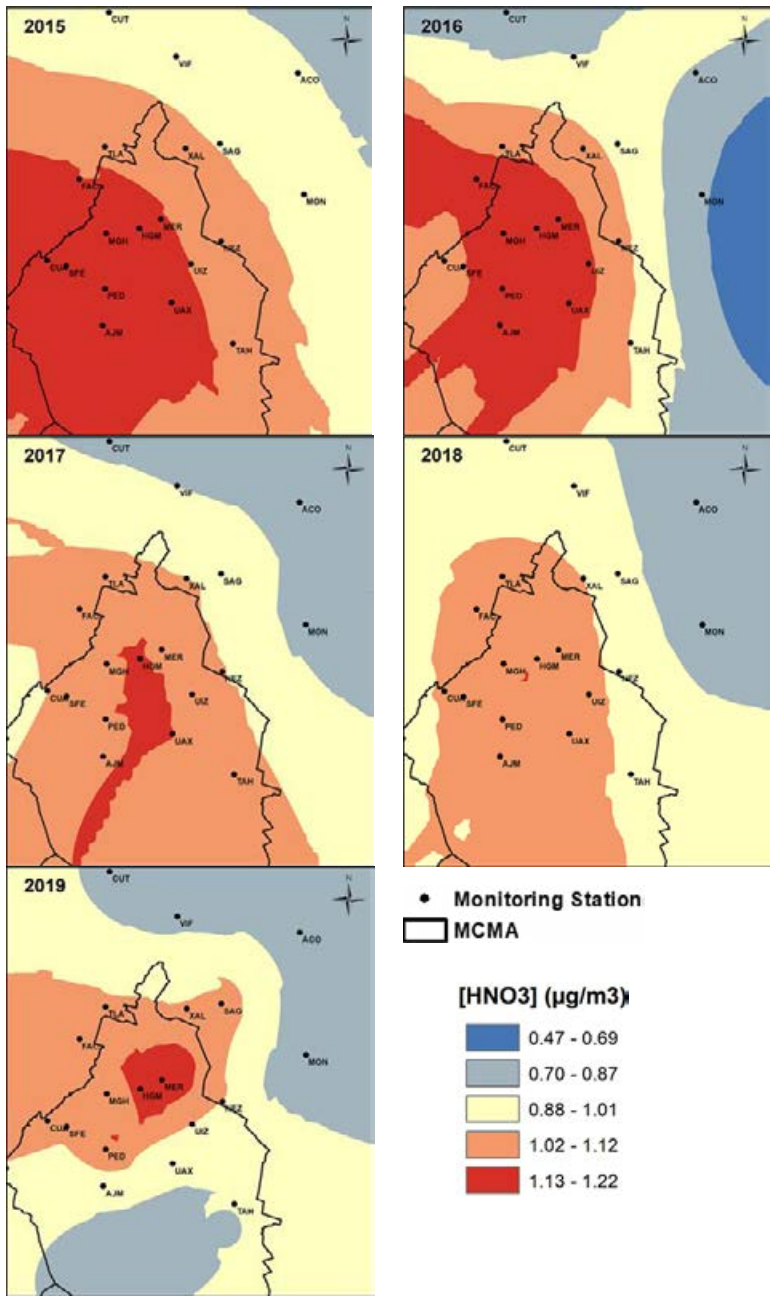

Fig. 3: Maps of concentration layers of the annual average of [HNO_3] ($\mu g/m^3$) for the period 2015-2019 in the MCMA

corrosion rates present in 2015 and 2016, while the lowest corrosion rate occurred in 2019. The highest corrosion rates are presented in the years 2015 and 2016. It is probably due to the high levels of [HNO_3] observed in Fig. 3. In contrast, the lowest corrosion rate occurred in 2019. The above is probably due to both sulfur dioxide and nitrogen dioxide, which present the lowest concentration levels in the 2015-2019 period. However, the fact that the corrosion rate for 2019 is the lowest in magnitude compared

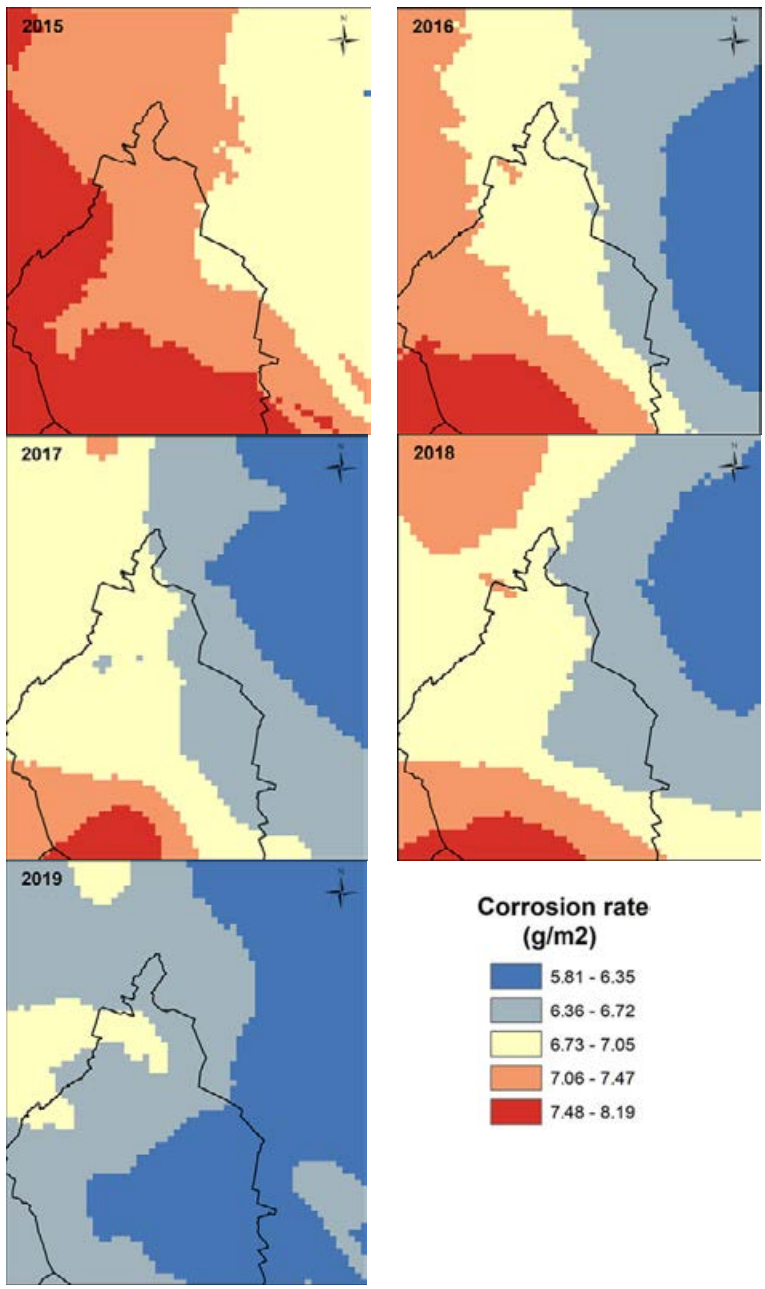

Fig. 4: Corrosion rate maps (g/m^2) of zinc, for a multi-pollutant situation for the period 2015-2019 in the MCMA

to other years, in percentage terms, has a significant influence on the corrosion rate for this year. The low perdetermination coefficient values R^2 were obtained mainly in constructing the climatic parameters' layers, possibly due to the nature and variability of the data obtained from the monitoring networks. The HNO_3 percentage contribution layers to the annual zinc corrosion rate are shown in Fig. 6. The impact is determined by combining the layers of corrosion rates of Figs. 4 and 5 in a percentage relationship

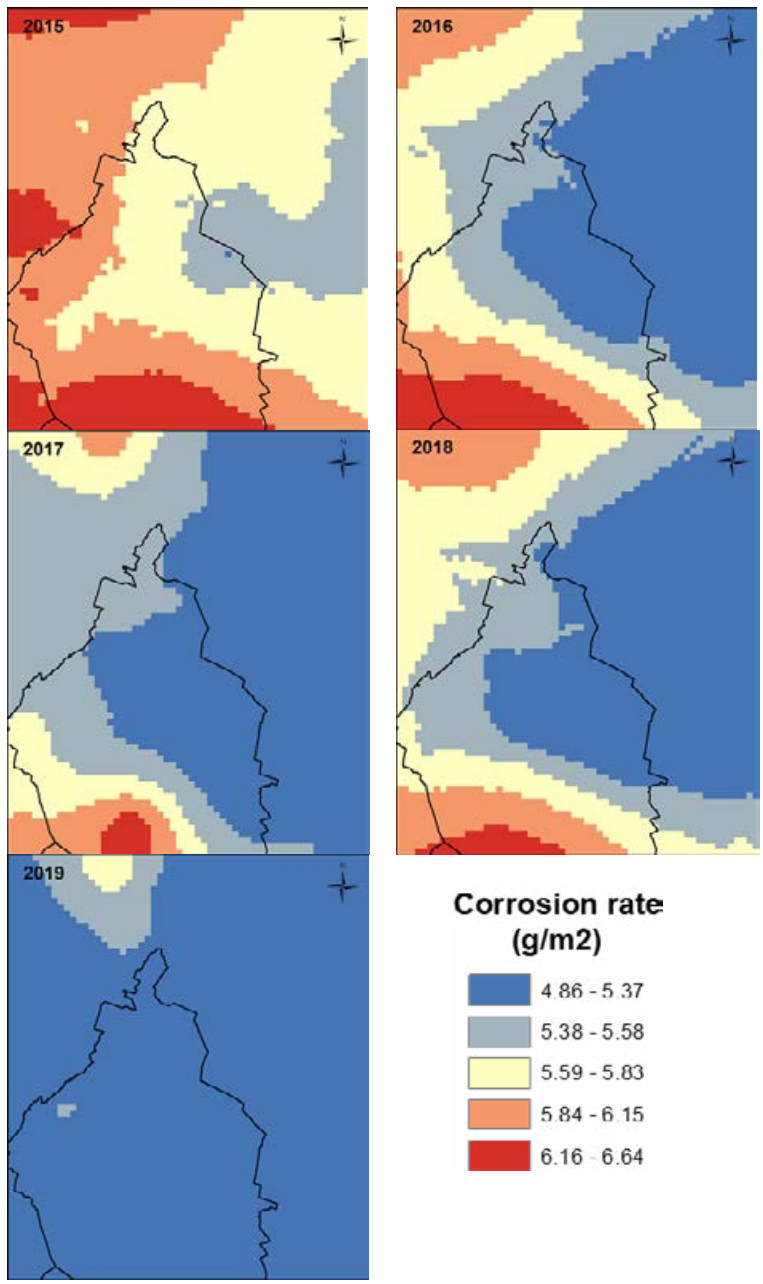

Fig. 5: Corrosion rate maps (g/m²) of zinc, for a multi-pollutant situation without the HNO_3 component for the period 2015-2019 in the MCMA

for 2015-2019. The images indicate a % contribution interval of 12.23-32.15. Spatially, the areas with the greatest contribution are located in the "center", and the areas with the least contribution are to the "east" of the MCMA. Temporarily the areas with the highest contribution are presented in the years 2015, 2016, and 2019. This is mainly due to the decrease in [SO_2] levels and the oxidation process of NO_2 to HNO_3 that occurs in the complex urban atmosphere of the MCMA, while the areas with the lowest contribution

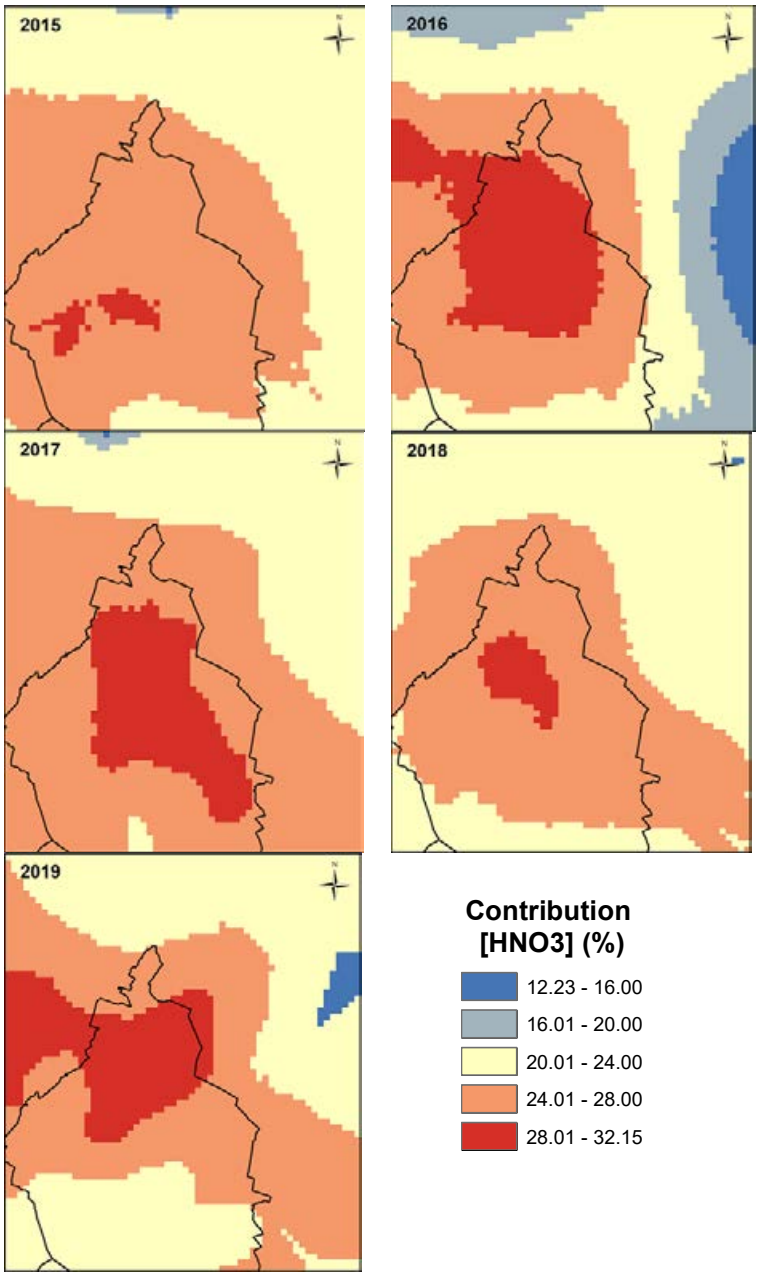

Fig. 6: Maps of the contribution (%) of HNO_3 to the annual zinc corrosion rate (g/m^2) of zinc, for a multi-pollutant situation for the 2015-2019 period in the MCMA

Table 2 Environmental data including temperature (T), relative humidity (RH), precipitation (Rain and pH) and gaseous pollutants (HNO_3 and SO_2). (Tidblad *et al.*, 2007)

Country	Test site name	SO_2 ($\mu g/m^3$)	Temperature (°C)	Relative humidity (%)	Rain (mm)	pH	HNO_3 ($\mu g/m^3$)
India	Bhubaneswar-u	4	26.5	69	425	6.0	1.3
India	Bhubaneswar-r	3	26.5	69	425	6.0	1
Thailand	Bangkok	11	29.3	76	1,371	6.8	2.3
Thailand	Phrapradaeng	59	29.3	73	1,335	6.2	1.5
Vietnam	Hanoi	15	24.7	79	1,556	5.8	0.8
Vietnam	Ho Chi Minh	21	28.3	74	1,441	6.2	0.9
Vietnam	Mytho	2	27	81	1,222	6.4	0.3
China	Chongqing	99	18.5	70	1,162	4.5	1.3
China	Tie Shan Ping	51	18.5	90	1,133	4.2	1.8
China	Hong Kong	16	22.9	78	2,092	4.6	1.8
Malaysia	Kuala Lumpur	12	28	78	2,776	4.3	3.8
Malaysia	Tanah Rata	0	18.1	91	2,433	5.1	0.1
South Africa	Johannesburg	18	17.2	78	417	4.8	2.1
Zambia	Kitwe	92	22.6	58	1,083	4.7	0.9
Zambia	Magoye	0	22.2	62	826	7.0	0.5
Zimbabwe	Harare	16	18.9	63	798	6.6	0.7

Table 3. Estimation of the % contribution of HNO_3 to the zinc corrosion rate (g/m^2) for different test sites

Country	Test site name	ML (g/m^2) of zinc, for a multi-pollutant situation	ML (g/m^2) of zinc, for a multi-pollutant situation without the HNO_3 component	Contribution % HNO_3
Malaysia	Tanah Rata	4.46	4.32	3.17
Vietnam	Mytho	5.61	5.20	7.90
Zimbabwe	Harare	6.73	5.77	16.61
Zambia	Kitwe	8.43	7.19	17.14
Vietnam	Hanoi	7.33	6.23	17.58
Zambia	Magoye	4.22	3.53	19.39
China	Chongqing	10.63	8.85	20.12
Vietnam	Ho Chi Minh	7.17	5.94	20.75
China	Tie Shan Ping	13.66	11.19	22.04
India	Bhubaneswar−r	6.39	5.02	27.31
China	Hong Kong	10.84	8.38	29.44
Thailand	Phrapradaeng	8.49	6.43	31.96
India	Bhubaneswar−u	6.89	5.11	34.84
South Africa	Johannesburg	9.79	6.91	41.61
Malaysia	Kuala Lumpur	16.71	11.50	45.25
Thailand	Bangkok	8.78	5.63	55.98

% are located in the year 2016. The difference is due to the annual concentration levels of HNO_3 compared to SO_2 and the other climatic parameters of the dose-response function.

On the other hand, in the latitudinal position of the MCMA, solar radiation is intense and accelerates photochemical reactions of pollutants in the atmosphere such as ozone and aerosols. Since ozone is involved in the formation of nitric acid, empirical equation 3 derived for other conditions must be reevaluated. There are limitations modeling atmospheric corrosion by empirical equations obtained in other situations. For example, in many cases, the weather when the exposure starts is relevant. It is different to start an atmospheric exposure in summer than in winter. Also, using annual mean temperature values for the MCMA has temperatures below 10 °C for many periods throughout the year. This effect is probably related to the time of wetness (TOW), an important variable that is not explicitly

considered in the MULTI- ASSESS equation. Table 2 shows gaseous pollutant and environmental data from a network of test sites that includes 12 sites in Asia (India, Vietnam, Thailand, Malaysia, and China, including Hong Kong) and four test sites in Africa (South Africa, Zambia, and Zimbabwe). Implemented by the RAPIDC program and funded by the Swedish International Development Agency (SIDA), in order to obtain corrosion values for materials including zinc after one year of exposure (2002-2003) (Tidblad *et al.,* 2007).

Table 3 shows the estimate of the % contribution of HNO_3 to the zinc corrosion rate (g/m^2). This is possible, using the values from Table 2 in equation 2 and combining in a percentage relationship the corrosion rate (g/m^2) of zinc in a multi-pollutant situation with the multi-pollutant situation without the HNO_3 component. Table 3 shows a contribution interval % HNO_3 of 3.17 - 55.98 with a great difference in the climatic and pollution values of the test sites. Johannesburg 41.61%, Kuala Lumpur 45.25% and Bangkok 55.98% show the highest HNO_3 contribution % values corresponding to the highest measured HNO_3 values. While Tanah Rata 3.17% and Mytho 7.90% have the lowest % contribution values of HNO_3 in relation to the lowest values of HNO_3 measured.

Comparing the interval of % contribution of HNO_3 of 12.23-32.15 observed in fig. 6 with the interval of values of 3.17-55.98 of Table 3, it is highlighted that it is possible to place it at an intermediate level with respect to the values of Table 3. However, the values in Table 3 are from more than a decade ago; there was already evidence of a significant contribution % of HNO_3 to the zinc corrosion process. However, at that time there was an important attention to SO_2.

CONCLUSION

Most studies on atmospheric zinc corrosion and galvanized steel carried out in Mexico and the Mexico City Metropolitan Area have focused on contaminants such as sulfur dioxide and sodium chloride, coupled with meteorological factors such as those responsible for damage to urban infrastructure and objects made of zinc or galvanized Steel. This work estimates nitric acid's contribution to zinc corrosion in the Mexico City Metropolitan Area. This contribution is represented as a component that includes HNO_3 in the dose-response functions for a multi-pollutant situation. In the multi-pollutant case, other factors also intervene, such as sulfur dioxide, relative humidity, amount of precipitation, temperature, and the acidity of the rain. The construction of corrosion rate maps using dose-response functions for a multi-pollutant situation in equation (2) provides a spatial and temporal estimate of the variation in corrosion rates in 2015-2019. This estimate allows visualizing areas where zinc materials are at risk corrosion due to the dispersion of atmospheric pollutants and climatic parameters. The construction of percentage maps shows the contribution (%) of HNO_3. HNO_3 contributes at least 12% and up to 32% to the zinc corrosion rate. These layers show that the years 2015, 2016, and 2019 present the highest contribution percentages. The equation (2) is applicable in geographic areas without the influence of chlorides and countries with tropical and subtropical climates, characteristic of the MCMA. Therefore, it is likely that the corrosion rate values obtained with the multi-pollutant dose-response function in this work are overestimated. It is desirable to have specific multi-pollutant dose-response functions for the MCMA that adequately represent the dispersion of pollutants and climatic parameters of the study area's urban atmosphere. It would be possible to implement an Exposure Program on the effects of atmospheric zinc corrosion, with specific attention to HNO_3. There is a relatively good correlation between the extrapolated loss of zinc mass resulting from laboratory exposures and the dose-response function based on statistical analysis. Therefore, the corrosion rates estimated for zinc in this work are very likely to represent an approximate value of the corrosion rates for zinc that can be found in field tests. This due to the absence of field tests.

AUTHOR CONTRIBUTIONS

J.O. Castillo-Miranda conceived the original idea, performed the literature review, analyzed and interpreted the data, prepared the manuscript text, and manuscript edition. F.J. Rodríguez-Gómez worked out the technical details, analyzed and interpreted the data, prepared the manuscript text, and manuscript edition. J. Genescá-Llongueras encouraged to investigate a specific aspect, helped in the literature review and manuscript preparation. L.G. Ruiz-Suárez developed the theoretical formalism and supervised the findings of this work. J.A. García-Reynoso helped shape the study, analysis and contributed to the interpretation of the results.

ACKNOWLEDGMENTS

J.O. Castillo-Miranda is grateful to "PROGRAMA DE BECAS POSDOCTORALES UNAM-DGAPA" for the postdoctoral scholarship and the authors (J.O. Castillo-Miranda and F.J. Rodríguez-Gómez) would like to thank the UNAM Facultad de Química, Departamento de Ingeniería Metalurgica. The authors want to acknowledge the contribution of Carlos Arroyave, Professor Emeritus University of Antioquia and Dr. Farid Samie, Shell Global Solutions, Houston Texas, USA (TA2 Materials and Corrosion Engineering).

CONFLICT OF INTEREST

The authors declare no potential conflict of interest regarding the publication of this work. In addition, the ethical issues including plagiarism, informed consent, misconduct, data fabrication and, or falsification, double publication and, or submission, and redundancy have been completely witnessed by the authors.

ABBREVIATIONS

%	Percentage
°C	Degree Celsius
µg/L	Micrograms per liter
µg/m^3	Micrograms per cubic meter
ArcGIS	Aeronautical reconnaissance coverage Geographic Information System
Ca^{2+}	Calcium ion
Cl$^-$	Chlorides
CLRTAP	Long-range Transboundary Air Pollution
cm/s	Centimeters per second
CO_2	Carbon dioxide
DGAPA-UNAM	Dirección General de Asuntos del Personal Académico de la Universidad Nacional Autónoma de México
EMEP	European Monitoring and Evaluation Materials Program
Eq.	Equation
Fig.	Figure
FTIR	Fourier transform spectroscopy
g/m^2	Grams per square meter
GIS	Geographic information systems
h/y	Hour per year
H$^+$	Hydrogen ion
H_2O	Water
H_2S	Hydrogen sulfide
HCl	Hydrogen chloride
HNO_3	Nitric acid
ICP materials	Co-operative programme on effects on materials, including historic and cultural monuments
IDW	Inverse distance weighting
ISO	International Organization for Standardization
ISOCORRAG	The International Testing Program
ISO/TC 156	International Organization for Standardization/Technical Committees 156
K$^+$	Potassium ion
km	Kilometres
m/s	Meters per second
MCMA	Mexico City Metropolitan Area
mg/L	Milligrams per liter
mg/m^2/day	Milligrams per square meter day
Mg/y	Megagrams per year
MICAT	Ibero-American Map of Atmospheric Corrosiveness
ML	Corrosion rate
mm	Millimeters
mmHg	Milimeters of mercury
mol/L atm	Mole per liter atmosphere
MULTI-ASSESS	Model for multi-pollutant impact and assessment of threshold levels for cultural heritage
Na$^+$	Sodium ion
NO_2	Nitrogen dioxide
NO_3^-	Nitrate ion
NOx	Nitrogen oxides
O_3	Ozone
pH	Hydrogen potential
PP	Precipitation or rain
ppb	Parts per billon
ppm	Parts per million
R^2	Coefficient of determination
Rain	Amount of precipitation
RAMA	Automatic Atmospheric Monitoring Network
RAPIDC	Regional Air Pollution in Developing Countries

REDDA	Atmospheric Deposit Network
REDMET	Atmospheric Monitoring Network and the Meteorology and Solar Radiation Network
RH	Relative humidity
RMS	Root Mean Square
RMSE	Least mean square error
SD	Standard deviation
SIDA	Swedish International Development Agency
SO_2	Sulfur dioxide
SUV	Sport utility vehicle
T	Temperature
TOW	Time of Wetness
UN ECE	Convention of the United Nations Economic Commissions for Europe
V_d	Deposition rate
$Zn(NO_3)_2$	Zinc nitrate
$Zn_5(NO_3)_2(OH)_8 \bullet 2H_2O$	Basic nitrate o essential nitrate

REFERENCES

ArcGIS, (2014). Software ArcGIS ArcMap Version 10.2.2. Environmental Systems Research Institute (ESRI). New York, USA.

Avila, D., (2018). Influencia de las condiciones meteorológicas en el depósito atmosférico húmedo en la Zona Metropolitana de la Ciudad de México. Tesis, Programa de Maestría en Ingeniería Ambiental – Aire. UNAM. **(131 pages).**

Báez, P.A.; Belmont, D.R.; García, R.M.; Torres, M.C.B.; Padilla, H.G., (2006). Rainwater chemical composition at two sites in Central. Atmos. Res., 80: 67–85 **(19 pages).**

Castillo-Miranda, J.O.; Torres-Jardón, R.; García-Reynoso, J.A.; Mar-Morales, B.E.; Rodríguez- Gómez, F.J.; Ruiz-Suárez, L.G., (2017). Mapping recession risk for cultural heritage stone In Mexico City due to dry and wet deposition of urban air pollutants. Atmósfera 30(3): 189-207 **(19 pages).**

CONAGUA, (2019). Coordinación General del Servicio Meteorológico Nacional de la Comisión Nacional del Agua (CONAGUA), 2019. El reporte del clima en México. Reporte anual 2019. Subgerencia de climatología y servicios climáticos y el área de vinculación e información climatológica y meteorológica **(79 pages).**

Conesa, G.C., (1996). Areas de aplicación medioambientales de los 'SIG'. Modelización y avances recientes. Papeles de Geografía. 23-24: 101-115 **(15 pages).**

Cuevas, J.A., (2014). Correlación entre ácido nítrico gaseoso y ozono en un sitio receptor de smog fotoquímico de la Ciudad de México. Tesis, Posgrado en Ciencias de la Tierra (Maestría). UNAM. **(88 pages)**.

Dean Jr., S.H., (2005). Atmospheric. In: Corrosion test and standards: Aplication and interpretation (R. Baboian Ed). ASTM International. 159-169 **(11 pages)**.

Denby, B.; Horálek, J.; Walker, S.; Eben, K; Fiala, J., (2005). Interpolation and assimilation methods for European scale air quality assessment and mapping, part 1: Review and recommendations. Europ. Topic Centre Air Climate Change. 14-18 **(5 pages).**

Denby, B.; Sundvor, I.; Cassiani, M.; De Smet, P.; De Leeuw, P.; Horálek, J., (2010). Spatial mapping of ozone and SO_2 trends in Europe. Sci. Total Environ, 408(20): 4795-4806 **(12 pages).**

Diem J.E.; Comrie, A.C., (2002). Predictive mapping of air pollution involving sparse spatial observations. Environ. Pollut., 119(1): 99-117 **(19 pages).**

Edney, E.O.; Stiles, D.C.; Spence, J.W.; Haynie, H.; Wilson, W.E., (1986). A Laboratory study to evaluate the impact of NOx, SOx, and oxidants on atmospheric corrosion of galvanized Steel, in: Materials degradation caused by acid rain: developed from the 20th state-of-the-art symposium of the American Chemical Society. Baboian, R., Editor. ACS Symposium 318, ACS, Washington, DC. 172-193 **(22 pages).**

Edney, E.O.; Stiles, D.C., (1986). Laboratory investigations of the impact of dry deposition of SO_2 and wet deposition of acidic species on the atmospheric corrosion of galvanized Steel. Atmos. Environ., 20(3): 541–548 **(8 pages).**

Ferm, M.; De Santis, F.; Varotsos, C., (2005). Nitric acid measurements in connection with corrosion studies. Atmos. Environ., 39(35): 6664–6672 **(9 pages).**

Finlayson-Pitts, B.J.; Pitts Jr., J.N., (2000). Chemistry of the upper and lower atmosphere theory, experiments, and applications. Academic Press. **(969 pages).**

Friel, J.J., (1986). Atmospheric corrosion products on Al, Zn, and AlZn metallic coatings. Corrosion, 42(7): 422-426 **(5 pages).**

García, R.; Belmont, R.; Padilla, H.; Torres, Ma. del C.; Baez, A.P., (2009). Determination of inorganic ions and trace elements in total suspended particles at three urban zones in the Mexico City Metropolitan Area and one rural site. Atmos. Res., 94(2): 313–319 **(7 pages).**

Genescá, J.; Rodriguez, C., (1992). Calibracion de la agresividad de la atmósfera del suroeste de la Ciudad de México, Rev. Int. Contam. Ambient. 8(2): 81-90 **(10 pages).**

Graedel, T.E.; Schwartz, N., (1977). Air quality reference data for corrosion assessment, Mater. Perform., 16(8): 17-25 **(9 pages).**

Graedel, T.E., (1989). Corrosion mechanisms for zinc exposed to the atmosphere. J. Electrochem. Soc., 136(4):193C-203C **(11 pages).**

Graedel, T.E.; Frankenthal, R.P., (1990). Corrosion mechanism for iron and low steels exposed to the atmosphere. J. Electrochem. Soc., 137(8): 2385-2394 **(10 pages).**

Guttman, H.; Sereda, P.J., (1968). Measurement of atmospheric factors affecting the corrosion of metals. Metal corrosion in the atmospheres, ASTM STP 435, ASTM International, West Conshohocken, PA, 326-359 **(34 pages).**

Hamilton, R.; Crabbe, H., (2009). Chapter 1 Environment, Pollution and effects, In: The effects of air pollution on cultural heritage. Watt, J., Tidblad, J., Kucera, V., Hamilton, R. (Editors). Springer. 1-27 **(27 pages)**.

INEGI, (2007). Instituto nacional de estadística, geografía e historia. Anuario estadístico de los Estados Unidos Mexicanos. Edición 2007 **(158 pages).**

Jáuregui, O.E., (2000). El clima de la Ciudad de México, Temas selectos de geografía de México. Plaza y Valdés. México, D.F. **(133 pages).**

Jáuregui, E.; Romales E., (1996). Urban effects on convective precipitation in Mexico city. Atmos. Environ., 30(20): 3383-3389 **(7 pages).**

Johansson, L.G., (1990). Synergistic effects of air pollutants on the

atmospheric corrosion of metals and calcareous stones. Ma. Chem., 30: 113-122 **(10 pages).**

Knotková, D.; Bartoň, K., (1992). Effects of acid deposition on corrosion of metals. Atmos. Environ., 26ª(17): 3169 3177 **(9 pages)**.

Knotková, D., (1993). Atmospheric corrosivity classification. Results from the international testing program ISOCORRAG, Corrosion control for low-cost reliability, 12th international corrosion congress, progress industries plant operations, NACE international, Houston, Texas. 2: 561–568 **(8 pages).**

Knotková, D.; Kreislova, K., (2007). Chapter 3: Corrosivity of atmospheres – derivation and use of information, In: Environmental deterioration of materials. Editor: Moncmanová, A., WIT Press. 73-102 **(30 pages).**

Kucera, V.; Fitz, S., (1995). Direct and indirect air pollution effects on materials including cultural monuments. Water Air Soil pollut., 85: 153-165 **(13 pages).**

Kucera, V., (2003). Changing pollution situation and its effect on material corrosion, In: Effects of air pollution on cultural heritage and its mitigation. Cultural heritage research: a Pan-European challenge. Proceedings of the 5th EC conference, May 16-18, 2002, Cracow, Poland, 23-29 **(7 pages).**

Kucera, V., (2004). Mapping of effects on materials ICP materials, In: Manual on methodologies and criteria for Modelling and Mapping Critical Loads and Levels and Air Pollution Effects, Risks and Trends, IV·1-IV·9 **(9 pages).**

Kucera, V., (2005). EU 5FP RTD Project model multi-pollutant impact and assessment of threshold levels for cultural heritage, final report **(52 pages).**

Kucera, V.; Tidblad, J.; Kreislova, K.; Knotkova, D.; Faller, M.; Reiss, D.; Snethlage, R.; Yates, T.; Henriksen, J.; Schreiner, M.; Melcher, M.; Ferm, M., Lefèvre, R-A.; Kobus, J., (2007). UN/ECE ICP Materials: Dose-response functions for the multi-pollutant situation, Water, Air Soil Pollut., 7(1): 249-258 **(10 pages).**

Leuenberger-Minger, A.U.; Faller, M.; Richner, P., (2002). Runoff of copper and zinc caused by atmospheric corrosion, Mater Corros., 53(3): 157–164 **(8 pages).**

Mariaca, L.; Genescá, J.; Uruchurtu, J.; Hernandez, L.S., (1999). Corrosividad atmosférica (MICAT-MÉXICO). Plaza y Valdes, **(209 pages)**.

Molina, L.T.; Molina, M.J., (2002). Air quality in the Mexico megacity (an integrate assessment); Kluwer Academic Publishers. 33-35 **(3 pages).**

Moreno, A., (2006a). Los sistemas de información geográfica. Una breve presentación, En: Sistemas y análisis de la información geográfica (A. Moreno, Coordinador) Editorial Ra-ma, 3-17 **(15 pages)**.

Moreno, A., (2006b). Las capas raster conceptos básicos, tipos de tratamientos y visualización. En: Sistemas y análisis de la información geográfica (A. Moreno, Coordinador) Editorial Ra-ma, 587-598 **(12 pages).**

Moya, M.; Grutter, M.; Baez, A., (2004). Diurnal variability of size differentiated inorganic aerosols and their gas phase precursors during january and february of 2003 near downtown Mexico City. Atmos. Environ., 38(33): 5651–5661 **(11 pages).**

Muñoz, L.R.; Uruchurtu, C.J., (2002). Caracterización de la agresividad atmosférica sobre los materiales metalicos estructurales en la zona metropolitana de la ciudad de México. Revista internacional de contaminación ambiental, 18(001), Universidad Nacional Autónoma de México, 27-32 **(6 pages).**

Oesch, S., (1996). Effect of SO_2, NO_2, NO and O_3 on the corrosión of unalloyed carbon steel and weathering Steel - the results of laboratory exposures. Corrosion Sci., 38(8): 1357–1368 **(12 pages).**

Oesch, S.; Faller, M., (1997). Environmental effects on materials: the effect of the air pollutants SO_2, NO_2, NO and O_3 on the corrosion of copper, zinc and aluminium. A short literature survey and results of laboratory exposures. Corrosion Sci., 39(9): 1505-1530 **(26 pages).**

Pantani, M.; Sabbioni, C.; Bruzzi, L.; Manco, D., (1998). Air pollution deposition on stones of artistic interest. Trans. Ecol. Environ., 21: 675-684 **(10 pages).**

Phillips, L.D.; Marks, G.D., (1996). Spatial uncertainty analysis: propagation of interpolation errors in spatially distributed models. Ecol. Model., 91(1-3): 213-229 **(17 pages).**

Roberge, P.R.; Klassen, R.D.; Haberecht, P.W., (2002). Atmospheric corrosivity modeling-a review. Mater. Des., 23(3): 321-330 **(10 pages).**

Rojas-Avellaneda, D., (2007). Spatial interpolation techniques for estimating levels of pollutant concentrations in the atmosphere. Revista Mexicana de Física. 53(6): 447-454 **(8 pages).**

Samie, F.; Tidblad, J.; Kucera, V.; Leygraf, C., (2007a). Atmospheric corrosion effects of HNO_3 a comparison of laboratory and field exposed copper, zinc, and carbon steel. J. Electrochem. Soc., 154(5): C249-C254 **(6 pages).**

Samie, F.; Tidblad J.; Kucera, V.; Leygraf, C., (2007b). Atmospheric corrosion effects of HNO_3—Comparison of laboratory-exposed copper, zinc and carbon steel. Atmos. Environ., 41(23): 4888–4896 **(9 pages)**.

SEDEMA, (2016). Secretaría del medio ambiente de la ciudad de México (SEDEMA), 2016. Calidad del aire en la ciudad de México, informe 2015. Dirección general de gestión de la calidad del aire, Dirección de monitoreo atmosférico. México, D. F. Julio.

SEDEMA, (2017). Secretaría del medio ambiente de la ciudad de México (SEDEMA), 2017. Calidad del aire en la ciudad de México, informe 2016. Dirección General de Gestión de la Calidad del Aire, Dirección de monitoreo atmosférico. Ciudad de México.

SEDEMA, (2018a). Secretaría del medio ambiente de la ciudad de México (SEDEMA), 2018. Inventario de emisiones de la ciudad de México 2016. Dirección general de gestión de la calidad del aire, Dirección de programas de calidad del aire e inventario de emisiones. Ciudad de México. Septiembre 2018.

SEDEMA, (2018b). Secretaría del medio ambiente de la ciudad de México (SEDEMA), 2018. Calidad del aire en la ciudad de México, informe 2017. Dirección general de gestión de la calidad del aire, Dirección de monitoreo atmosférico. Ciudad de México. Octubre.

SEDEMA, (2018c). Secretaría del medio ambiente de la ciudad de México (SEDEMA), 2018. Calidad del aire en la ciudad de México, informe 2017. Dirección general de gestión de la calidad del aire, Dirección de monitoreo atmosférico. Ciudad de México. Octubre.

SEDEMA, (2020a). Calidad del aire. Secretaria del Medio Ambiente del Gobierno de la Ciudad de México. Recovered 20200728.

SEDEMA, (2020b). Secretaría del medio ambiente de la ciudad de México (SEDEMA), 2020. Calidad del aire en la ciudad de México, Informe 2018. Dirección general de calidad del aire, Dirección de Monitoreo de Calidad del Aire.

SEDEMA, (2020c). Calidad del aire. Secretaria del Medio Ambiente del Gobierno de la Ciudad de México. Recovered 20210418.

Seinfeld J.H.; S.N. Pandis, (2016). Atmospheric chemistry and physics from air pollution to climate change. Jonh Wiley and Sons. **(1226 pages).**

Seinfeld, J.H., (1980). Lectures in Atmospheric Chemistry. Am. Insti-

tute Chem. Eng., 12(76), **(98 pages).**
SMA, (2008). Secretaría del Medio Ambiente del Gobierno del Distrito Federal. Informe de la Calidad del Aire en la Zona metropolitana del valle de México, Estados y tendencias 1990-2007 **(50 pages).**
Spence, J.W.; Haynie, F.H., (1990). Derivation of a damage function for galvanized steel structures: corrosion kinetics and thermodynamic considerations," in Corrosion testing and evaluation: Silver Anniversary Volume, ed. R. Baboian and S. Dean (West Conshohocken, PA: ASTM International); 208-224 **(17 pages)**.
Svensson, J.E.; Johansson, L.G., (1993). A laboratory study of the initial stages of the atmospheric corrosion of zinc in the presence of NaCl; influence of SO_2 and NO_2. Corrosion Sci., 34(5): 721-740 **(20 pages).**
Tidblad, J.; Kucera, V.; Mikhailov, A.A.; Henriksen, J.; Kreislova, K.; Yates, T.; Stöckle, B.; Schreiner, M., (2001). UN ECE ICP Materials: Dose-response functions on dry and wet acid deposition effects after 8 years of exposure. Water, Air Soil Pollut., 130: 1457-1462 **(6 pages).**
Tidblad, J.; Kucera, V.; Mikhailov, A.A.; Henriksen, J.; Kreislova, K.; Yates, T.; Singer, B., (2002a). "Field exposure results on trends in atmospheric corrosion and pollution," Outdoor atmospheric corrosion, ASTM STP 1421, H. E. Townsend, Ed., American society for testing and materials international, West Conshohocken, PA. **(14 pages).**
Tidblad, J.; Kucera, V.; Mikhailov, A.A.; Knotkova, D., (2002b). "Improvement of the ISO classification system based on dose-response functions describing the corrosivity of outdoor atmospheres," Outdoor Atmospheric Corrosion, ASTMSTP 1421, H.E. Townsend, Ed., American Society for Testing and Materials International, West Conshohocken, PA. **(15 pages).**
Tidblad, J.; Kucera, V.; Samie, F.; Das, S.N.; Bhamornsut, C.; Peng, L.C.; Lung So, K.; Dawei, Z.; Hong Lien, L.T.; Schollenberger, H.; Lungu, C. V.; Simbi, D., (2007). Exposure programme on atmospheric corrosion effects of acidifying pollutants in tropical and subtropical climates, Water Air Soil Pollut., 7: 241–247 **(7 pages).**
Tidblad, J.; Kucera, V.; Sherwood, S., (2009). Chapter 3: Corrosion, In: The effects of air pollution on cultural heritage. Watt, J.; Tidblad, J.; Kucera, V.; Hamilton, R. (Editors), Springer. 53-103 **(51 pages).**
Tidblad J.; Kucera, V.; Ferm, M.; Kreislova, K.; Brüggerhoff, S.; Doytchinov, S.; Screpanti, A.; Grøntoft, T.; Yates, T.; De la Fuente, D.; Roots, O.; Lombardo, T.; Simon, S.; Faller, M.; Kwiatkowski, L.; Kobus, J.; Varotsos, C.; Tzanis, C.; Krage, L.; Schreiner, M.; Melcher, M.; Grancharov, I.; Karmanova, N.; (2012). Effects of air pollution on materials and cultural heritage: ICP Materials celebrates 25 years of research. Int. J. Corrosion. 2012, Article ID 496321 **(16 pages).**
UN, (2016). The world's cities in 2016 – Data booklet (ST/ESA/SER.A/392). United Nations, Department of Economic and Social Affairs, Population Division.
Venkatram, A., (1988). On the use of kriging in the spatial analysis of acid precipitation data. Atmos. Environ., 22(9): 1963-1975 **(13 pages).**
Wood, E.C.; Herndon, S.C.; Onasch, T.B.; Kroll, J.H.; Canagaratna, M.R.; Kolb, C.E.; Worsnop, D.R.; Neuman, J.A.; Seila, R.; Zavala, M.W.; Knighton, B., (2009). A case study of ozone production, nitrogen oxides, and the radical budget in Mexico City, Atmos. Chem. Phys., 9: 2499-2516 **(17 pages)**.
Zeiler, M., (1999). Modeling our world The ESRI guide to geodatabase design. Environmental systems research institute, Inc. 2-4, 24-27, 46-47 **(2 pages)**.
Zheng, J.; Zhang, R.; Fortner, E.C.; Volkamer, R.M.; Molina, L.; Aiken, A.C.; Jimenez, J.L.; Gaeggeler, K.; Dommen, J.; Dusanter, S.; Stevens, P.S.; Tie, X., (2008). Measurements of HNO_3 and N_2O_5 using ion drift-chemical ionization mass spectrometry during the MILAGRO/MCMA-2006 campaign. Atmos. Chem. Phys., 8: 6823-6838 **(16 pages).**

AUTHOR (S) BIOSKETCHES

Castillo-Miranda, J.O., Ph.D., Postdoctoral stay, Departamento de Ingeniería Metalúrgica, Facultad de Química, Universidad Nacional Autónoma de México, Circuito Exterior s/n, Ciudad Universitaria, C.P. 04510, Ciudad de México, México.
Email: *j9lechatelier@yahoo.com.mx*

Rodríguez-Gómez, F.J., Ph.D., Professor, Departamento de Ingeniería Metalúrgica, Facultad de Química, Universidad Nacional Autónoma de México, Circuito Exterior s/n, Ciudad Universitaria, C.P. 04510, Ciudad de México, México. Email: *fxavier@unam.mx*

Genescá-Llongueras, J., Ph.D., Professor, Polo Universitario de Tecnología Avanzada, Universidad Nacional Autónoma de México, Vía de la Innovación 410 PIIT Autopista Monterrey-Aeropuerto Km. 10 C.P. 66629, Apodaca, Nuevo León, México.
Email: *genesca@unam.mx*

Ruiz-Suárez, L.G., Ph.D., Professor, Centro de Ciencias de la Atmósfera, Universidad Nacional Autónoma de México, Circuito de la Investigación Cientifica, Ciudad Universitaria, C.P. 04510, Ciudad de México, México. Email: *ruizs@unam.mx*

García-Reynoso, J.A., Ph.D., Professor, Centro de Ciencias de la Atmósfera, Universidad Nacional Autónoma de México, Circuito de la Investigación Cientifica, Ciudad Universitaria, C.P. 04510, Ciudad de México, México. Email: *agustin@atmosfera.unam.mx*

HOW TO CITE THIS ARTICLE

Castillo-Miranda, J.O.; Rodríguez-Gómez, F.J.; Genescá-Llongueras, J.; Ruiz-Suárez, L.G.; García-Reynoso, J.A., (2021). Estimation and mapping of the contribution of nitric acid to atmospheric corrosion of zinc. Global J. Environ. Sci. Manage., 7(4): 523-542.

DOI: 10.22034/gjesm.2021.04.03

url: https://www.gjesm.net/article_243716.html